Screening effect in electromagnetic production of electron-positron pairs in relativistic nucleus-atom collisions

Jianshi Wu,[1] J. H. Derrickson,[2] T. A. Parnell,[2] and M. R. Strayer[3]
[1]*Department of Natural Sciences, Fayetteville State University, Fayetteville, North Carolina 28301*
[2]*NASA/Marshall Space Flight Center, Huntsville, Alabama 35812*
[3]*Physics Division, Oak Ridge National Laboratory, Oak Ridge, Tennessee 37831*
(Received 19 April 1999)

We study the screening effects of the atomic electrons in the electromagnetic production of electron-positron pairs in relativistic nucleus-atom collisions for fixed target experiments. Our results are contrasted with those obtained in bare collisions, with particular attention given to its dependence on the beam energy and the target atom. [S1050-2947(99)06311-8]

PACS number(s): 34.90.+q, 25.75.−q, 23.20.−g

I. INTRODUCTION

The electromagnetic production of electron-positron pairs along heavy ion tracks has been extensively studied theoretically since the 1930s [1–3] and experimentally since the 1950s [4–6]. The construction of the new colliders, the Relativistic Heavy-Ion Collider (RHIC) at Brookhaven National Laboratory and the Large Hadron Collider (LHC) at CERN, has renewed interest in the electromagnetic production of electron-positron pairs and other particles in ultrarelativistic heavy ion collisions [7–10]. Numerous numerical calculations of pair production in nucleus-nucleus collisions have been done over the past decade using both perturbative and nonperturbative methods. It is anticipated that predictions from lowest-order perturbative theory might fail for heavy colliding systems and at high impact energies. Theoretical treatments for higher-order perturbative expansions have been developed by several authors [11–15]. They all found that multiple pair creation probability can be written in the form of a Poisson distribution, which restores unitarity. The recent measurements of electron-positron pairs [16,17] provided notable agreements and differences with predictions of lowest-order perturbation calculations. It was pointed out [10,17] that one of the sources for the differences might be the screening effect of the target atom in the measured colliding system. Comparisons with predictions in theory should be made with calculations which include the effects of screening on the fields.

More recently, use of the electromagnetic production of electron-positron pairs has been proposed by various authors for the energy measurements of ultrarelativistic heavy ions [18,19] in the cosmic ray studies, since the direct process of pair production is purely electromagnetic and the pair yield does not saturate at high energies. In the practical design of a direct electron pair detector, the cross section, or the yield of pairs, is used to measure the energy of the cosmic rays. Here, it is also essential to include the screening effects of the atomic electrons in the target atom in pair production and some background sources such as the production of knock-on electrons in the simulations. It is the purpose of the present paper to report the study on the atomic screening effects on pair production in detail.

II. CLASSICAL FIELD APPROXIMATION

We follow the model [20] previously developed for particle production induced by colliding ultrarelativistic nuclei. In this model, the sharply peaked electromagnetic fields near the nuclei are approximated by their classical counterparts, and the coherent production mechanism is treated as the excitations of quantum fields using perturbation theory. For the lowest-order processes the cross section of pair production can be written as a Feynman integral in momentum space, and carried out numerically using the Monte Carlo method [8]. Here, we shall extend our existing formalism to also include a form factor which accounts for the charge distribution of the electron cloud around the nucleus.

We start at the interaction picture in the quantum field theory with a Hamiltonian density to describe the interaction between the particle fields and the radiation field $A_\mu(x)$. The classical field model is obtained by replacing $A_\mu(x)$ by their classical counterparts. The electromagnetic potentials arising from the motion of two colliding nuclei are

$$A^\mu(x)=A_a^\mu(x)+A_b^\mu(x), \tag{1}$$

where a and b label the nuclei. These potentials can be calculated from the nuclear charge density in the local rest frame of each nucleus, and then boosted to the center-of-velocity frame.

In the center-of-velocity frame of $a+b$, the potentials in momentum space are given by

$$A_{a,b}^\mu(q)=2\pi Z_{a,b}e\,\delta(q^0\mp\beta q^z)f_{a,b}(q)\exp(\pm i\vec{q}_\perp\cdot\vec{b}/2)u_{a,b}^\mu, \tag{2}$$

where $\vec{b}$ is the impact parameter which displaces the trajectories of two nuclei as shown in Fig. 1, $q=\sqrt{-q^\mu q_\mu}$ and q_μ is the four-momentum transfer, and

$$u_{a,b}^\mu=(1,0,0,\beta) \tag{3}$$

are the ''boost'' four velocities. $f(q)$ can be written in terms of the invariant form factor $F(q)$ for the charge distribution

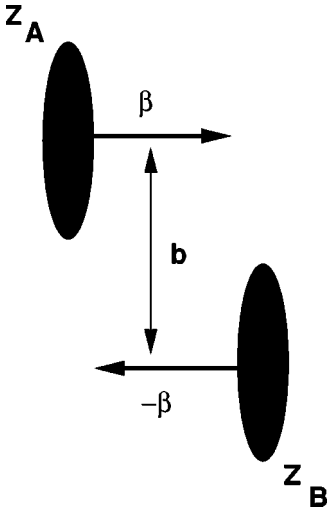

FIG. 1. Schematic diagram depicting a relativistic collision of two charges Z_A and Z_B, in the center-of-velocity frame with impact parameter b and velocity β.

$$f(q)=\frac{1}{q^2}F(q). \tag{4}$$

Here, the screening effects can be explicitly introduced in the target atom by using the atomic form factor arising from the charge distribution of the electron cloud around the nucleus.

Since the electromagnetic fields are treated as *c*-number fields, they can be factored out from the evaluation of the *S*-matrix element with Feynman rules applying to the remaining part of the calculation. The total cross section is obtained by integration over the impact parameter and summing over all final states

$$\sigma=\int d^2b\sum_f |\langle f|S|0\rangle|^2. \tag{5}$$

In our calculation the *S*-matrix element is obtained from the second-order processes as shown in the Feynman diagrams in Fig. 2. After carrying out the integration over the impact parameter, we obtain the cross section

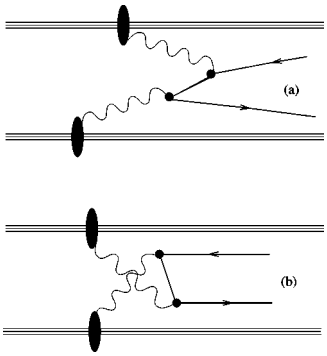

FIG. 2. Shown are the lowest-order Feynman diagrams for electron-positron pair production in heavy-ion collisions: (a) direct diagram and (b) exchange diagram.

$$\begin{aligned}\sigma_{ab\to e^+e^-}&=\int\frac{d^3k_1d^3k_2}{(2\pi)^6 2E_1 2E_2}\int d^2b\sum_{s_1,s_2}|\langle\vec{k}_1s_1\vec{k}_2s_2|S^{(2)}|0\rangle|^2\\&=\frac{Z_a^2Z_b^2(4\pi\alpha)^4}{4\beta^2}\int\frac{d^3k_1d^3k_2d^2q_{a\perp}}{(2\pi)^8 2E_1 2E_2}\\&\quad\times f_a^2(q_a)f_b^2(q_b)\sum_{s_1,s_2}\left|\overline{u}(\vec{k}_1,s_1)\left\{\not{u}_a\frac{1}{\not{k}-m}\not{u}_b+\not{u}_b\frac{1}{\not{k}'-m}\not{u}_a\right\}v(\vec{k}_2,s_2)\right|^2.\end{aligned} \tag{6}$$

The integral is carried out numerically using the Monte Carlo method. The advantage of Monte Carlo integration is that the standard error in the calculation can be followed to the desired precision, and all the distributions of produced particles can be accumulated while the total cross section is carried out.

III. ATOMIC FORM FACTOR

It is a general approach to the screening effect to introduce an atomic form factor to the nucleus [21] using the Thomas-Fermi approximation [22].

Generally, for a spherical charge distribution the normalized form factor $F(q)$ is given by

$$F(q)=\frac{4\pi}{Zeq}\int_0^\infty rdr\,\sin(qr)\rho(r), \tag{7}$$

where $\rho(r)$ is the charge density.

For a neutral atom the atomic form factor can be written as

$$f(q)=\frac{1}{q^2}[F_N(q)-F_e(q)], \tag{8}$$

where $F_N(q)$ and $F_e(q)$ are the form factors due to the nuclear and electronic charge distributions, respectively.

The analytical representations of atomic potentials have been proposed by many authors [23]. Most such attempts have made use of analytic approximations to the statistical model of Thomas-Fermi. In the simplest form of the theory, the potential of a neutral atom is taken as

$$V(r)=-Ze\phi_{\rm TF}(x)/r, \tag{9}$$

where $x=rZ^{1/3}/\mu_0$ is dimensionless, and $\mu_0=\frac{1}{2}(3\pi/4)^{2/3}(\hbar^2/m_ee^2)\approx 0.8853\ (\hbar^2/m_ee^2)$, and the screening function $\phi_{\rm TF}(x)$ satisfies the dimensionless Thomas-Fermi equation

$$x^{1/2}\frac{d^2\phi_{\rm TF}(x)}{dx^2}=[\phi_{\rm TF}(x)]^{3/2}. \tag{10}$$

In the usual treatment, the screening function satisfies $\phi_{\rm TF}(0)=1$ and $\phi_{\rm TF}(x)\to 0$ as $x\to\infty$. Equation (10) can be solved numerically. However, for the purpose of Monte

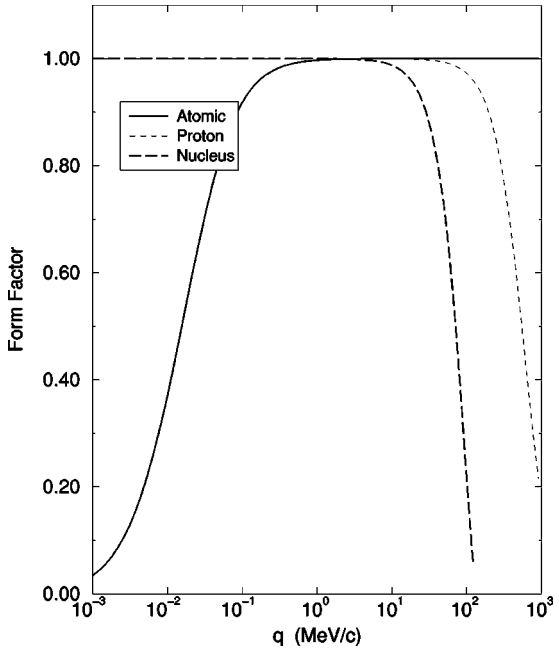

FIG. 3. Depicted are the form factors as a function of q. The full line is for the screening form factor $1-F_e(q)$ of electrons in the neutral atom of ^{208}Pb, the dashed line is for the form factor of the nucleus ^{208}Pb, and the dotted line is for the form factor of a proton.

Carlo integration an analytical form factor is preferred. We choose the form suggested by Teitz [24],

$$\phi_T(x)=\left[1+\left(\frac{\pi}{8}\right)^{2/3}x\right]^{-2}, \tag{11}$$

which works very well over a wide range of x. The electron charge density $\rho_e(r)$ is written in terms of the Thomas-Fermi function as

$$\rho_e(r)=\frac{e}{4\pi}\left[\frac{Z}{\mu_0 r}\phi_{\mathrm{TF}}\left(\frac{rZ^{1/3}}{\mu_0}\right)\right]^{3/2}. \tag{12}$$

The analytical form of the form factor using the Teitz function $\phi_T(x)$ as an approximation can be expressed in terms of the incomplete gamma function,

$$F_e(q)=\frac{1}{Q}\mathrm{Im}\{G(Q)\}, \tag{13}$$

where $Q=qb/Z^{1/3}$, $a=(\pi/8)^{2/3}$, and

$$G(Q)=\sqrt{\frac{\pi}{a}}\left\{e^{-i(Q/a)}\Gamma\left(\frac{1}{2},-i\frac{Q}{a}\right)\left(\frac{3}{8}-\frac{Q^2}{2a^2}+i\frac{Q}{2a}\right)-\left[\frac{3\sqrt{2}}{8}\left(\frac{Q}{a}\right)^{1/2}+\frac{\sqrt{2}}{4}\left(\frac{Q}{a}\right)^{3/2}\right]\right\}. \tag{14}$$

Here $\Gamma(\alpha,z)$ is the incomplete gamma function. The details of the derivation and the numerical scheme for calculating the incomplete gamma function are discussed in the Appendix. Figure 3 gives a numerical comparison between $1-F_e(q)$ and $F_N(q)$ for ^{208}Pb, where the proton form factor $F_p(q)$ is also shown for comparison. Since the regions where $1-F_e(q)$ and $F_N(q)$ are significantly different from 1 do not overlap, it is a good approximation to factorize the atomic form factor into the product of $1-F_e(q)$ and $F_N(q)$, i.e.,

$$f(q)=\frac{1}{q^2}F_N(q)[1-F_e(q)]. \tag{15}$$

The way we introduce the atomic form factor for the screening effect agrees with Refs. [25] and [10] except for its specific analytical form that we chose.

IV. RESULTS AND DISCUSSION

We carried out the Feynman integral of the total cross section for electron-positron pair production in nucleus-atom collisions for various colliding systems and beam energies using Monte Carlo integration. The results are compared with the total cross section for nucleus-nucleus collisions for the same nuclei at the same energies. Table I shows the comparison for Au-Au collisions at beam energies in the target frame ranging from 200 GeV/n to 200 TeV/n. The total cross section increases dramatically with the beam energy. The total cross section for pair production in nucleus-nucleus collisions goes up asymptotically [8] as $[\ln(\gamma)]^3$, where the γ factor represents the beam energy in the center-of-velocity frame. This behavior can be understood since two $\ln(\gamma)$ factors account for the boost of the virtual photon flux carried by each nucleus, and the other $\ln(\gamma)$ factor is from the photon-photon cross section. The reduction of the cross section due to screening in the atom also increases with the beam energy and rises from less than 5% to more than 30% as the beam energy is raised from 200 GeV/n to 200 TeV/n. This can also be understood from the boost of the photon flux. The screening due to the electrons tends to reduce the flux of the low momentum virtual photons in the rest frame of the nucleus, and, therefore, the boosted virtual photon flux for the atom is much reduced at high beam energies. It is

TABLE I. The total cross sections in units of barns for pair production in Au-Au collisions at various beam energies.

Beam energy (TeV/n)	Nucleus-atom	Nucleus-nucleus	Reduction
0.2	3.57×10^3	3.74×10^3	4.55%
2.0	1.22×10^4	1.41×10^4	13.5%
20	2.80×10^4	3.56×10^4	21.3%
200	4.82×10^4	7.03×10^4	31.4%

TABLE II. The total cross sections in units of barns for pair production at the beam energy of 20 TeV/n for different nuclei.

Colliding system	Nucleus-atom	Nucleus-nucleus	Reduction
Si-Si	29.7	35.2	15.6%
Ca-Ca	1.22×10^2	1.46×10^2	16.4%
Fe-Fe	3.45×10^2	4.18×10^2	17.5%
Au-Au	2.80×10^4	3.56×10^4	21.3%

seen that the total cross section for pair production is reduced accordingly.

Table II shows the total cross sections of pair production at a beam energy of 20 TeV/n for various colliding systems and the reduction due to screening. The cross section for nucleus-nucleus collisions goes up dramatically as Z^4, however the reduction due to screening increases only slightly with Z. The slight increase can be explained by the fact that the scale of the Thomas-Fermi distribution is inversely proportional to $Z^{1/3}$. The heavier the nucleus, the more screening in the atom at the same distance from the nucleus, and the $Z^{1/3}$ factor accounts for the weak Z dependence.

The Monte Carlo integration is performed in the center-of-velocity frame, while the observables are collected in the target frame after a Lorentz transformation. The probability for each Monte Carlo event is accumulated for all the distributions. Figure 4 shows the momentum spectra in the target frame for the produced positrons. The reduction due to screening is visible across the board in the spectrum, and the reduction is more significant at higher momenta.

Our calculations do show a significant reduction in the total cross section of electromagnetic production of electron-positron pairs, especially in the energy range of cosmic ray measurements, i.e., 1 TeV/n to 1000 TeV/n. Thus, it is essential to include the screening effect in the simulations for the energy measurement of cosmic rays in this energy range. As for the CERN experiments, the data were collected in beam-on-target experiments, and, therefore, we have to implement the screening effect in the calculation before we can really assess the discrepancy between theoretical results from the lowest-order Feynman diagrams and experimental data. The reduction at a beam energy around 200 GeV/n in the target frame may not be a very significant effect for the total cross section, especially for low-Z targets. However, the reduction in the high momentum spectrum needs to be investigated. Currently, we are repeating the detailed simulations with the screening effect implemented and the cutoffs on the Monte Carlo events defined according to the exact geometry in the detector used in the CERN experiments. We will report the comparison between theory and experiments in a future publication [26].

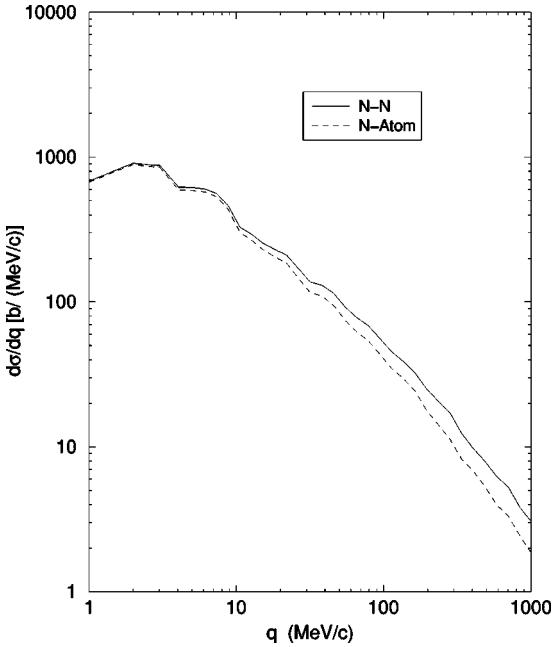

FIG. 4. Depicted are the momentum spectra of the produced pairs in the target frame for Au-Au collisions at a beam energy of 20 TeV/n. The full line is for the nucleus-nucleus collision and the dashed line is for the nucleus-atom collision.

ACKNOWLEDGMENTS

Partial support for this work was received from the following agencies: the National Aeronautics and Space Administration (NASA) under Grant No. NAG8-996 and the Marshall Space Flight Center under the Center Director's Discretionary Fund (CDDF) (Contract No. H-28521D), and the U.S. Department of Energy (DOE) under Grant Nos. DE-FG02-97ER41044 and DE-AC05-96OR22464 with Oak Ridge National Laboratory, managed by Lockheed Martin Energy Research Corporation. The numerical calculations were done on the CRAY T90 machine at the North Carolina Supercomputing Center and at the National Energy Research Supercomputing Center.

APPENDIX

If we define

$$g_\nu(Q,a)=\int_0^\infty \frac{1}{\sqrt{x}(1+ax)^\nu}e^{iQx}dx \tag{A1}$$

and

$$P(Q,\beta)=\int_0^\infty \frac{1}{\sqrt{x}(x+\beta)}e^{iQx}dx \tag{A2}$$

$$=\frac{\Gamma(1/2)}{\beta^{1/2}}e^{-iQ\beta}\Gamma(1/2,-iQ\beta), \tag{A3}$$

$g_1(Q,a)$ can be written as

$$g_1(Q,a)=\frac{1}{a}P(Q,1/a). \tag{A4}$$

It can be proved that the function $G(Q)$ is given by

$$G(Q)=g_3(Q,a) \tag{A5}$$

$$=\frac{1}{2}a^2\frac{\partial^2 g_1(x,a)}{\partial a^2}+2a\frac{\partial g_1(x,a)}{\partial a}+g_1(Q,a) \tag{A6}$$

$$= \sqrt{\frac{\pi}{a}}\left\{ e^{-i(Q/a)}\Gamma\left(\frac{1}{2}, -i\frac{Q}{a}\right)\left(\frac{3}{8} - \frac{Q^2}{2a^2} + i\frac{Q}{2a}\right) - \left[\frac{3\sqrt{2}}{8}\left(\frac{Q}{a}\right)^{1/2} + \frac{\sqrt{2}}{4}\left(\frac{Q}{a}\right)^{3/2}\right]\right\}. \quad \text{(A7)}$$

The incomplete gamma function $\Gamma(\frac{1}{2}, -ix)$ has to be programmed using different methods for different ranges of x values. We used the series expansion for $|x|<1$ and the continued fraction expansion for $|x|>1$ [27,28]. It is a numerical check for the code when the two different ways of calculation produce a perfect numerical match at the point $x=1$.

[1] C. F. von Weizsäcker, Z. Phys. **88**, 612 (1934).
[2] E. J. Williams, Proc. R. Soc. London, Ser. A **139**, 163 (1933).
[3] G. Racah, Nuovo Cimento **14**, 93 (1937).
[4] M. M. Block and D. T. King, Phys. Rev. **95**, 171 (1954); M. M. Block, D. T. King, and W. W. Wada, *ibid.* **96**, 1627 (1954).
[5] M. Koshiba and M. F. Kaplan, Phys. Rev. **97**, 193 (1955).
[6] J. E. Naugle and P. S. Freier, Phys. Rev. **104**, 804 (1956).
[7] G. Baur and C. A. Bertulani, Phys. Rev. C **35**, 836 (1987); C. A. Bertulani and G. Baur, Phys. Rep. **163**, 299 (1988).
[8] C. Bottcher and M. R. Strayer, Phys. Rev. D **39**, 1330 (1989).
[9] F. Decker, Phys. Rev. A **44**, 2883 (1991).
[10] P. B. Eby, Phys. Rev. A **39**, 2374 (1989); **43**, 2258 (1991); Nucl. Instrum. Methods Phys. Res. A **336**, 189 (1993).
[11] G. Baur, Phys. Rev. A **42**, 5736 (1990).
[12] M. J. Rhoades-Brown and J. Weneser, Phys. Rev. A **44**, 330 (1991).
[13] C. Best, W. Greiner, and G. Soff, Phys. Rev. A **46**, 261 (1992).
[14] M. C. Guclu, J. C. Wells, A. S. Umar, M. R. Strayer, and D. J. Ernst, Phys. Rev. A **51**, 1836 (1995).
[15] Adrain Alscher, Kai Hencken, Dirk Trautmann, and Gerhard Baur, Phys. Rev. A **55**, 396 (1997).
[16] C. R. Vane *et al.*, Phys. Rev. Lett. **69**, 1911 (1992); Phys. Rev. A **50**, 2313 (1994); **56**, 3682 (1997).
[17] J. H. Derrickson, P. B. Eby, K. H. Moon, T. A. Parnell, D. T. King, J. C. Gregory, Y. Takahashi, and T. Ogata, Phys. Rev. A **51**, 1253 (1995).
[18] Y. Takahashi, P. B. Eby, T. A. Parnell, J. C. Gregory, and T. Hayashi, in *Proceedings of the Workshop on Cosmic Ray and High Energy Gamma Ray Experiments for the Space Station Era, Baton Rouge, Louisiana, 1984*, edited by W. V. Jones and J. P. Wefel (Louisiana State University, Baton Rouge, 1985), p. 390.
[19] J. H. Derrickson, P. B. Eby, T. A. Parnell, Jianshi Wu, J. C. Gregory, and Y. Takahashi, in *Proceedings of the 24th International Cosmic Ray Conference, Rome, 1995*, edited by N. Iucci and E. Lamanna (Italian Society of Physics, Bologna, 1995), Vol. 3, p. 641.
[20] J.-S. Wu, C. Bottcher, and M. R. Strayer, Phys. Lett. B **252**, 37 (1990); J.-S. Wu, C. Bottcher, M. R. Strayer, and A. K. Kerman, Ann. Phys. (N.Y.) **210**, 402 (1991).
[21] A. Akhiezer and V. B. Berestetskii, *Quantum Electrodynamics* (Interscience, New York, 1965).
[22] L. D. Landau and E. M. Lifshitz, *Quantum Mechanics, Nonrelativistic Theory* (Addison-Wesley, Reading, MA, 1965).
[23] Alex E. S. Green, D. L. Sellin, and A. S. Zachor, Phys. Rev. **184**, 1 (1969).
[24] Von T. Teitz, Ann. Phys. (Leipzig) **15**, 186 (1955).
[25] S. R. Kelner, Sov. J. Nucl. Phys. **5**, 778 (1967).
[26] J. C. Wells, J.-S. Wu, J. H. Derrickson, T. A. Parnell, and M. R. Strayer (unpublished).
[27] I. S. Gradstein and I. M. Ryzhik, *Table of Integrals, Series, and Functions* (Academic, Boston, 1994).
[28] W. H. Press *et al.*, *Numerical Recipes* (Cambridge University Press, Cambridge, 1992).